

Local structure of Ge quantum dots determined by combined numerical analysis of EXAFS and XANES data

Yuanpeng Zhang,^{a*} Osman Ersoy,^a Ali Karatutlu,^{a,b} William Little^a and Andrei Sapelkin^a

Received 23 June 2015
Accepted 10 October 2015

^aSchool of Physics and Astronomy, Queen Mary, University of London, Mile End Road, London E1 4NS, UK, and
^bElectrical and Electronics Engineering, Yildirim Campus, Bursa Orhangazi University, 16245 Yildirim, Bursa, Turkey.
*Correspondence e-mail: yuanpeng.zhang@qmul.ac.uk

Edited by S. M. Heald, Argonne National Laboratory, USA

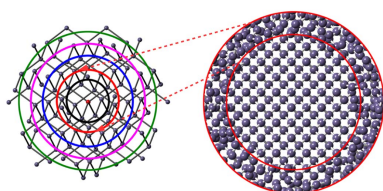
Keywords: XANES; EXAFS; FDMNES; Ge quantum dots; annealing; core-shell model.

Supporting information: this article has supporting information at journals.iucr.org/s

The sensitivity of X-ray absorption near-edge structure (XANES) to the local symmetry has been investigated in small (~ 4 nm) matrix-free Ge quantum dots. The *FDMNES* package was used to calculate the theoretical XANES spectra that were compared with the experimental data of as-prepared and annealed nanoparticles. It was found that XANES data for an as-prepared sample can only be adequately described if the second coordination shell of the diamond-type structural model is included in the *FDMNES* calculations. This is in contrast to the extended X-ray absorption fine-structure data that show only the first-shell signal. These results suggest that, despite the high degree of disorder and a large surface-to-volume ratio, as-prepared small Ge quantum dots retain the diamond-type symmetry beyond the first shell. Furthermore, we utilized this sensitivity of XANES to the local symmetry to study annealed Ge quantum dots and found evidence for significant structural distortion which we attribute to the existence of surface disorder in the annealed oxygen-free Ge quantum dots.

1. Introduction

Semiconductor quantum dots (QDs) are receiving increasing attention due to their tunable optical behaviour with the changing size or structure (Kim *et al.*, 2013; Lee *et al.*, 2009; Mao, 2013) and their potential for optical and biological application (Bruchez *et al.*, 1998; Kairdolf *et al.*, 2013; Michalet *et al.*, 2005; Pal, 2015; Peng, Long *et al.*, 2015). As a result, there has been extensive research into the properties of group III–V (*e.g.* InAs, GaAs) (Kabi & Perera, 2015; Uesugi *et al.*, 2015), group II–VI (*e.g.* CdSe, ZnS) (Bain & Ivanisevic, 2015; Peng, Sampat *et al.*, 2015; Zhou *et al.*, 2015) and group IV (C, Si) semiconductor quantum structures (Abualnaja *et al.*, 2015; Qian *et al.*, 2015; Wolf *et al.*, 2013; Zhang *et al.*, 2012). Another group IV semiconductor, Ge, a close structural and electronic analogue to Si, has received limited attention, but recently there has been significant interest in understanding the optical properties of Ge QDs (Barbaggiovanni *et al.*, 2014; Scarselli *et al.*, 2007; Sun, Sue *et al.*, 2005; Wheeler *et al.*, 2013; Little *et al.*, 2014). This interest has been fuelled in part by the recent development of relatively simple synthesis routes that enable matrix-free Ge QDs to be produced (Henderson *et al.*, 2010; Karatutlu *et al.*, 2015; Robel *et al.*, 2015; Wheeler *et al.*, 2013; Wong, 2009; Vaughn *et al.*, 2010). It has been shown that Ge QDs have a clear potential for application in infrared (IR) photo-detection to replace Pb-based IR detectors (Sanehira *et al.*, 2012). Furthermore, the low toxicity and tunable photo-



luminescence properties of Ge QDs indicate an exciting possibility for biological applications including cell imaging (Pellegrino *et al.*, 2005; Resch-Genger *et al.*, 2008), labelling (Michalet *et al.*, 2005) and photo-thermal therapy (Hope-Weeks, 2003; Vaughn *et al.*, 2010).

Information about the atomic structure of QDs is a prerequisite for understanding their electronic and optical properties since they can be greatly affected by the structure, morphology and surface state of nanoclusters (NCs) (Bera *et al.*, 2010; Lee *et al.*, 2009; Little *et al.*, 2014; Pizzagalli *et al.*, 2001; Weber *et al.*, 2013; Yakimov *et al.*, 2014). Such information also provides invaluable guidance in developing QDs synthesis routes that provide desired outcomes. However, characterizing ultra-small QDs (below ~ 10 nm) becomes challenging and often comes with a degree of uncertainty (Lu, 2012), due to significant surface, interface (Ferrer *et al.*, 2008; Weber *et al.*, 2013; Yuryev *et al.*, 2012) and size effects (Chiu *et al.*, 2006) and the effect of probes used to investigate sample structure (Chou *et al.*, 2009; Lv *et al.*, 2009; Marcins *et al.*, 2011; Ryu *et al.*, 2012; Wu *et al.*, 2011). In the case of Ge QDs, most samples prepared under mild colloidal synthesis conditions seem to be amorphous-like due to the relatively high crystallization temperature (Vaughn *et al.*, 2010). Thus the commonly used powder X-ray diffraction (PXRD) technique does not provide straightforward information for most as-prepared Ge QDs due to the lack of long-range order in samples. That, in some cases, makes it difficult to tell whether the as-prepared Ge QDs are completely amorphous or nanoclusters with small crystalline-domain (Muthuswamy *et al.*, 2013; Toko *et al.*, 2014; Zaitseva *et al.*, 2007). Electron microscopy too provides limited structural information with the added problem of sample annealing (Moore *et al.*, 1983; Tseng *et al.*, 1980) for amorphous-like samples. The situation is similar in Raman spectroscopy due to the possible laser annealing effects of amorphous-like samples (Lv *et al.*, 2009; Marcins *et al.*, 2011; Ryu *et al.*, 2012). Besides, it is not always straightforward to distinguish an amorphous Raman signal from that of very small nanoparticles. Hence, several reports show ambiguous structural results for as-prepared Ge QDs, obtained from PXRD (which shows an amorphous-like feature) and transmission electron microscopy (TEM; which shows a crystalline lattice plane) (Chou *et al.*, 2009; Wu *et al.*, 2011).

Under these circumstances X-ray absorption spectroscopy (XAS), which is sensitive to the local atomic arrangements, is a crucial source of complementary information. Indeed, the extended X-ray absorption fine structure (EXAFS) has been successfully used to describe the structure of nanoparticles in general (Cheng *et al.*, 2004; Frenkel, 1999; Rockenberger *et al.*, 1997; Sun *et al.*, 2006) and also of Ge QDs embedded into a SiO₂ matrix (Cosentino *et al.*, 2014; Kolobov, Oyanagi *et al.*, 2003; Kolobov *et al.*, 2001; Kolobov, Wei *et al.*, 2003; Sun, Wei *et al.*, 2005). Recently, we also reported application of the combination of short- and long-range order techniques to explore the structure and morphology of matrix-free Ge QDs (Zhang *et al.*, 2015) and to understand the origins of light emission (Little *et al.*, 2014).

While EXAFS is a powerful technique of choice for structural characterization of amorphous systems, it provides limited information about the local symmetry of disordered samples due to limited (usually to the first coordination shell) structural information. For characterizing QDs, there are added problems of complex nanoscale morphology (Ke *et al.*, 2015; Samavati, Mustafa *et al.*, 2015; Samavati, Othaman *et al.*, 2015; Sun *et al.*, 2015; Zhang *et al.*, 2014) and possible metastable phases (Chiu *et al.*, 2006; Nelmes *et al.*, 1993; Selli *et al.*, 2013) due to the small particle size and/or surface effects. At the same time, the near-edge portion of the XAS signal, *i.e.* the extended X-ray absorption near-edge structure (XANES; to around 50 eV above the absorption edge), is known to be very sensitive to medium-range order and electronic properties of samples (Norman, 1986; Pin *et al.*, 1989). The origin of this sensitivity is in the low kinetic energy of the photoelectron in the XANES region and hence relatively long electron mean free path (Newville, 2014; Penner-Hahn, 2002). This sensitivity has already been extensively used in chemistry, biology, catalysis and many other areas to selectively assess the oxidation state, local atomic symmetry, coordination, charge distribution, *etc.* of various atomic species (Asakura *et al.*, 2015; D'Angelo & Migliorati, 2015; Girod *et al.*, 2015; Hyun & Hayes, 2015; Jia *et al.*, 2014; Priebe *et al.*, 2015). Furthermore, the XANES signal has a much higher signal-to-noise ratio as compared with EXAFS and hence can be applicable, for example, to samples with lower concentrations (Newville, 2014). However, for most part such analysis has been qualitative and based on experimental standards owing to the complexity of information contained in XANES (Bunker, 2010). Recent developments of computational power and of the codes capable of sufficiently accurate XANES calculations make it possible to obtain quantitative structural and electronic information from experimental data.

Here we have utilized XANES to probe the structure beyond the first coordination shell in as-prepared Ge QDs. We also explored the influence of annealing on structural evolution. We show that XANES can provide key local symmetry information even in structurally disordered systems where EXAFS structural information is limited to the first coordination shell.

2. Methods

Ge QDs were synthesized through the reduction of GeCl₄ (256 ml) using NaBH₄ in a solution of ethylene glycol (10 ml), PVP (50 mg, MW = 630000) and triglyme (6 ml). The solution was then bubbled by using continuous Ar or H₂/Ar mixture gas with an inlet of a micro-tube through the solution. The final product was separated from the colloidal chemical solution by 10 min of centrifugation at 10000 r.p.m. In addition to the synthesis, the Ge QDs were annealed for 1 h in a H₂/Ar (mixture of H₂ and Ar) gas at a flow rate of 100 cc min⁻¹ at a temperature of 450°C. Samples were annealed immediately following synthesis and were sealed in glass capillaries (0.7 mm) immediately after annealing.

Transmission electron microscopy (TEM; Jeol 2010, acceleration voltage 200 kV, point-to-point resolution 1.94 Å) was employed to characterize the particle size distribution and morphology. The XAS measurement was carried out in transmission mode using ionization chambers, at Diamond Light Source (beamline B18, energy range: 10800–12400 eV with step-size 0.92 eV). Experimental EXAFS spectra were analysed using the *Demeter* package (Ravel *et al.*, 1995). The ‘Rbkg’ was set to 1.2 Å to prevent artificially suppressing possible Ge–O bonding signal. The default ‘Hanning’ window was used for the Fourier transform from *k*-space to *R*-space, and the *k*-range for the Fourier transform was as follows: Ge QDs sample (both as-prepared and annealed), 3–15 Å⁻¹; Dia-Ge Ref at room temperature, 2–14 Å⁻¹. For all the EXAFS spectra fitting, only the single scattering path was included. To extract the coordination number for our sample, the standard S_0^2 value was first obtained by fitting only the first shell of several EXAFS spectra of a diamond-type Ge reference measured at different temperatures (12 K, 200 K and 270 K). The overall average was then taken as the standard S_0^2 value. The fitted S_0^2 value was then compared with the standard value to extract the corresponding coordination number. The XANES spectra were calculated using the *FDMNES* package (Joly, 2001). In this article, the FDM (finite difference method) mode, which goes beyond the muffin-tin potential approximation (typically used for MS calculation) for solving the excited state, was used for the calculation of theoretical XANES spectra. The typical time scale for FDM mode

calculation, the parallel calculation using five nodes for a 7 Å diamond-type Ge cluster, takes 2–3 days.

3. Results and discussion

TEM images for both as-prepared and annealed Ge QDs are shown in Figs. 1(a) and 1(b). The QDs size distribution for each (obtained by randomly selecting 60 QDs for each set of samples) is given as the inset graph of Figs. 1(a) and 1(b). The average size calculated for as-prepared and annealed samples is 3.9 nm and 4.0 nm, respectively.

The magnitude of the Fourier transform (FT) of the background-subtracted EXAFS spectra and corresponding fitting (based on the diamond-type structure) for as-prepared and annealed Ge QDs are shown in Figs. 1(c) and 1(d), respectively. The fitted parameters are given in Table 1 together with those for diamond-type Ge reference [to evaluate the quality of the EXAFS spectra, the $\chi(k)$ data are provided in the supporting information]. One can see that neither as-prepared nor annealed Ge QDs show signal, above the noise level, corresponding to the Ge–O bond (the theoretical Ge–O bond length is ~ 1.78 Å; Bolzan *et al.*, 1997). This confirms that sealing of samples in glass tubes following synthesis and annealing did prevent oxidation. The low value of the first-shell coordination number (~ 3.5 ; Table 1) for as-prepared and annealed samples should be attributed to the large surface-to-volume ratio due to the small size of the QDs. Furthermore, for the as-prepared sample we only observe signal corre-

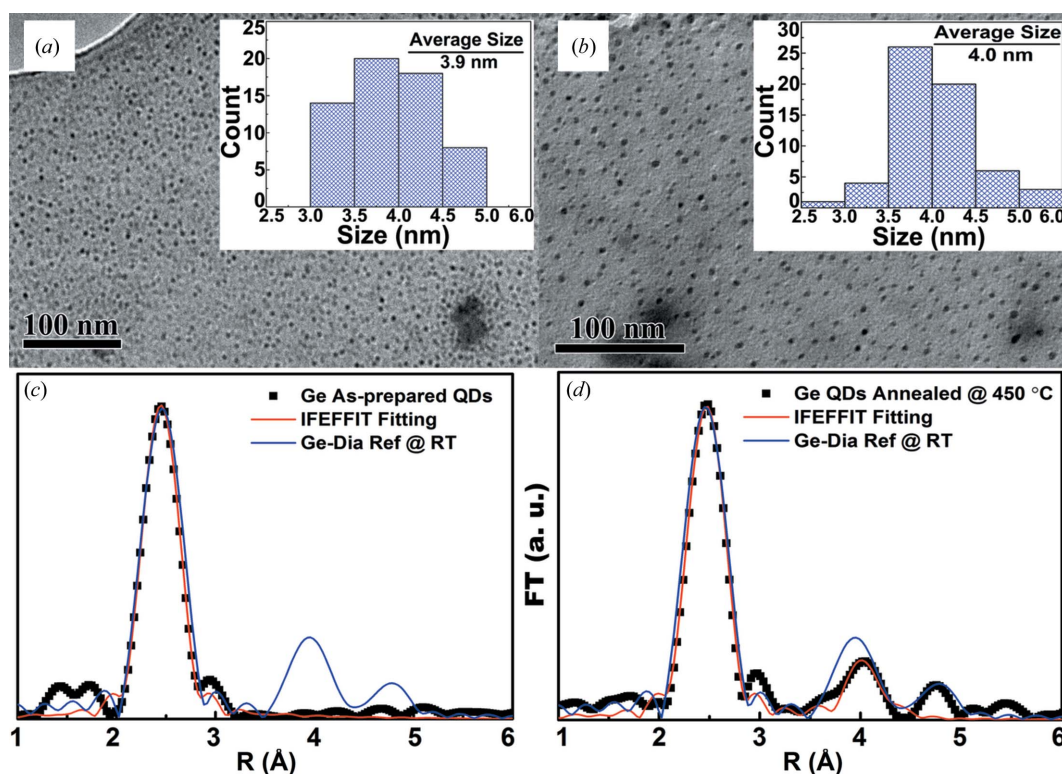


Figure 1

(a, b) TEM and size distribution obtained for as-prepared (a) and annealed (b) Ge QDs. (c, d) Experimental and fitted magnitude of the Fourier transform of the EXAFS signal for the as-prepared (c) and annealed (d) sample. The data for diamond-type bulk Ge [measured at room temperature (RT)] are also given.

Table 1

Fitting result for experimental EXAFS spectra of as-prepared and annealed Ge QDs.

The corresponding standard value for the diamond-type Ge reference is also given for comparison. The value of E_0 was kept the same for all samples (11097.5 eV).

	R (Å)	DW factor (Å ²)	Coordination number	S_0^2
As-prepared	2.43 (1)	0.0052 (2)	3.5 (1)	0.94
Annealed	2.45 (1)	0.0051 (3)	3.5 (1)	0.94
	4.01 (2)	0.020 (3)	10.5 (3)	0.94
Reference – amorphous†	2.46	0.0054 (1)	3.9	NA
Reference – diamond	2.45	0.0036 (1)†	4.0	0.94 (2)
	4.00	0.008 (2)‡	12	NA

† Filippini & Di Cicco (1995). ‡ Stern *et al.* (1983).

sponding to the first Ge–Ge coordination shell, indicating that no long-range order exists. The reduced Ge–Ge bonding length (~ 2.43 Å; Table 1) and a large value of the corresponding Debye–Waller (DW) factor value (~ 0.005 Å²; Table 1) also imply structural distortion as compared with diamond-type Ge. For the annealed sample [see Fig. 1(d)] the fitted Ge–Ge bond lengths (first shell: ~ 2.45 Å; second shell: ~ 4.01 Å) are close to those found in standard diamond-type Ge. However, both the first- and second-shell DW factors (see Table 1) are larger than that of the diamond-type Ge reference. Particularly for the second shell, the DW factor for the annealed sample is more than double that of the reference.

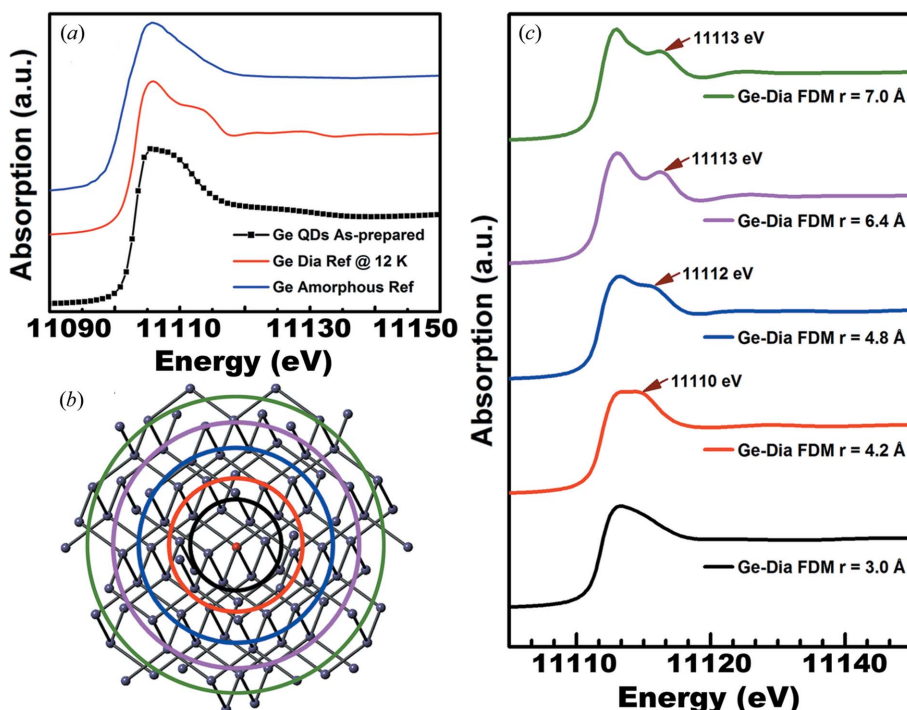


Figure 2
 (a) Comparison of XANES spectra for as-prepared Ge QDs, amorphous Ge (Backman *et al.*, 2009) and bulk diamond-type Ge. (b) Illustration of the calculation cluster including different local coordination shells. (c) Simulated XANES spectra for diamond-type Ge structure by FDMNES using FDM mode, where the calculation cluster size was set from 3.0 Å to 7.0 Å. The arrows indicate the second main feature position in each spectrum.

This indicates significant distortion in the second shell, which may correspond to variations in the bonding angle.

Thus, EXAFS analysis suggests that as-prepared samples are most likely amorphous. However, comparison of XANES spectra shown in Fig. 2(a) clearly shows that signal from as-prepared Ge QDs is neither identical to that of bulk diamond-type Ge reference nor to that of a typical amorphous Ge film (Backman *et al.*, 2009). Therefore, to further explore the origins of these differences in the XANES spectra we focused on an in-depth XANES analysis.

For diamond-type Ge structure, the calculation cluster radius was set to a series of values from 3.0 Å up to 7.0 Å (Fig. 2b) to simulate the change in the local order effects on the XANES signal. The results are shown in Fig. 2(c). When only the first shell was included ($r = 3.0$ Å), the simulated XANES spectrum is featureless, which is consistent with the experimental spectra for amorphous Ge (see Fig. 2a). When the second shell was included ($r = 4.2$ Å), the second main feature [labelled with arrows in Fig. 2(c)] appears close to the white line. Furthermore, with the increasing of cluster size, the position of this second feature [obtained by analysing the second derivative of the spectrum (see the supporting information)] shifts to higher energy reaching 11113 eV for a cluster radius of ~ 7.0 Å.

By directly comparing our calculations with the XANES spectra of as-prepared Ge QDs (see Fig. 3) we found that all the main features (designated as A, B and C around the region labelled by the rectangle) in the experimental spectra can be

successfully reproduced only when two coordination shells (cluster size $r = 4.2$ Å) are included in the calculation. The analysis here thus shows that inclusion of a second shell is required to adequately reproduce the XANES of the as-prepared sample. This is something that is not at all obvious from the EXAFS data and shows that XANES analysis shows a detectable degree of local ordering in as-prepared Ge QDs beyond the first coordination shell. This is consistent with our previous analysis (Zhang *et al.*, 2015) of the powder X-ray diffraction pattern for an as-prepared sample, which shows a narrower diffraction peak compared with a typical amorphous Ge signal. This means that XANES can be used to provide local symmetry information in small nanoparticles when EXAFS data are limited to the first shell only.

We then turned our attention to annealed samples. The positions of several features (marked by vertical dashed lines) just above the absorption edge for our annealed Ge QDs are shown in Fig. 4, designated as A, B and C. By comparison with the XANES of

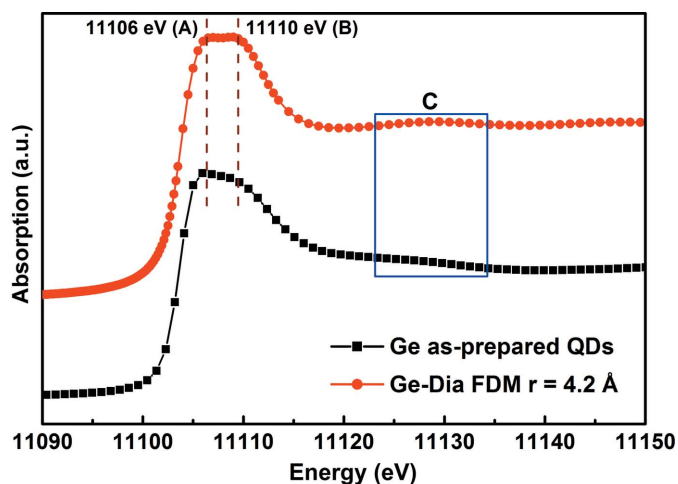


Figure 3
Comparison of experimental XANES spectra of as-prepared Ge QDs with simulation, for which only the first two shells are included in the calculation cluster (radius $r = 4.2$ Å) using FDM mode.

the diamond-type Ge reference, it can be seen that our annealed Ge QDs show an extra feature at around 11110 eV (designated as B; Fig. 4). The positions of the other two features (A and C) are identical to the reference. By comparing Figs. 3 and 4, one can see that the positions of features B are identical (~ 11110 eV; Figs. 3 and 4) in both cases. This suggests similar structural origins of these features in as-prepared and annealed samples. This, together with the theoretical XANES calculation shown in Figs. 2 and 3 and analysis for the as-prepared sample, indicates the presence of an amorphous-like component in the annealed Ge QDs with local order restricted to the first two coordination shells.

There are several possible scenarios for the structural configuration of annealed Ge QDs: (i) a mixture of fully crystalline diamond-type Ge QDs and those similar to the as-prepared Ge QDs (amorphous-like with local order to the second shell); (ii) a random distribution of crystalline and amorphous-like regions within a single Ge QD; (iii) a diamond-type crystalline core with an amorphous-like surface layer. The first case can be excluded on account of the EXAFS analysis of the annealed sample showing a second-shell DW value that is much larger than that of the reference (see Table 1), indicating larger disorder in the second coordination shell. At the same time, analysis of the as-prepared sample does not show a second-shell signal at all and thus cannot influence the overall second-shell DW. The second case, *i.e.* a mixed phase in a single QD with size down to sub-nanometers, can also be excluded on the basis of thermodynamic consideration (Weeks & Gilmer, 2007). Therefore, the most likely situation is the third case, *i.e.* the core-shell configuration in annealed Ge QDs (see inset in Fig. 4). This result is consistent with our previous analysis of EXAFS, optically detected XAS and molecule dynamics simulation, which shows the coexistence of diamond-type crystalline core and sub-nanometer amorphous surface layer in Ge QDs (Little *et al.*, 2014), and with first-principles and empirical molecular dynamics calculations (Pizzagalli & Galli, 2002).

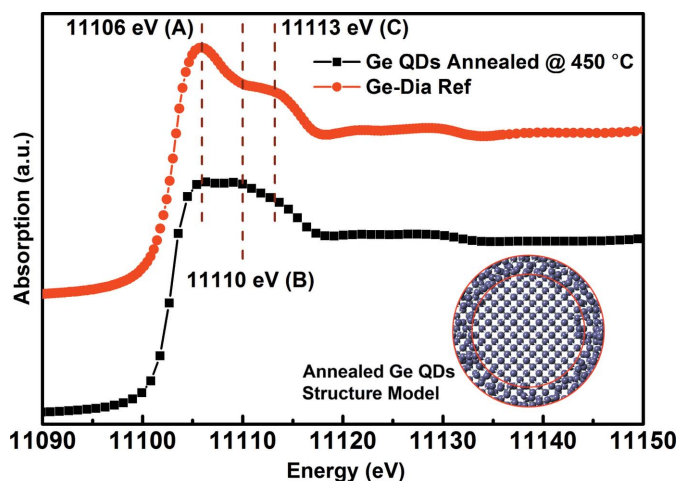


Figure 4
Position of features in the XANES spectra of annealed Ge QDs and the diamond-type Ge reference. The feature in the middle cannot be observed in the reference XANES spectrum. The positions were obtained by taking the derivatives of the XANES spectra. The inset is an illustration of the proposed core-shell model for annealed Ge QDs.

We thus conclude that as-prepared matrix-free colloidal Ge QDs show a high degree of structural disorder, but preserve local diamond-like symmetry. Annealing of as-prepared nanoparticles in an oxygen-free environment for 1 h at 450°C results in QDs crystallization, while surface disorder is still preserved.

4. Conclusion

The local structure of small (~ 4 nm) colloidal synthesized Ge QDs and of corresponding annealed samples was explored using X-ray absorption techniques. In all cases EXAFS shows no signal corresponding to Ge–O bonding. In as-prepared samples EXAFS data correspond to an amorphous-like structure, while in annealed samples a crystalline diamond-like structure is observed. Detailed XANES analysis clearly points to diamond-like local (up to 4.2 Å) symmetry in as-prepared samples; XANES analysis in annealed samples points to core-shell-like particle morphology with crystalline core and a disordered shell. This clearly shows that XANES can provide key supplementary information about the local coordination environment when EXAFS data are limited to the first shell only. The results here imply that, for the reconstruction of atomic-level structure in nanoparticles (including local symmetry), comprehensive quantitative analysis for both EXAFS and XANES spectra should be carried out.

Acknowledgements

This research utilized Queen Mary's MidPlus computational facilities, supported by QMUL Research-IT and funded by EPSRC grant EP/K000128/1. We would like to thank Diamond Light Source for the beamline (B18) and the experimental support from Konstantin Ignatyev, Giannantonio Cibin and Diego Gianolio *etc.* AK and OE acknowl-

edge the Turkish Ministry of National Education. YZ is grateful to the Chinese Scholarship Council (CSC) for financial support of his PhD study.

References

- Abualnaja, K. M., Šiller, L. & Horrocks, B. R. (2015). *Nanotechnology*, **26**, 145704.
- Asakura, H., Shishido, T., Teramura, K. & Tanaka, T. (2015). *J. Chem. Phys.* **142**, 164507.
- Backman, M., Djurabekova, F., Pakarinen, O. H., Nordlund, K., Araujo, L. L. & Ridgway, M. C. (2009). *Phys. Rev. B*, **80**, 144109.
- Bain, L. E. & Ivanisevic, A. (2015). *Small*, **11**, 768–780.
- Barbagniovanni, E. G., Lockwood, D. J., Simpson, P. J. & Goncharova, L. V. (2014). *Appl. Phys. Rev.* **1**, 011302.
- Bera, D., Qian, L., Tseng, T.-K. & Holloway, P. H. (2010). *Materials*, **3**, 2260–2345.
- Bolzan, A. A., Fong, C., Kennedy, B. J. & Howard, C. J. (1997). *Acta Cryst.* **B53**, 373–380.
- Bruchez, M., Moronne, M., Gin, P., Weiss, S. & Alivisatos, A. P. (1998). *Science*, **281**, 2013–2016.
- Bunker, G. (2010). *Introduction to XAFS: A Practical Guide to X-ray Absorption Fine Structure Spectroscopy*. Cambridge University Press.
- Cheng, G. J., Carter, J. D. & Guo, T. (2004). *Chem. Phys. Lett.* **400**, 122–127.
- Chiu, H. W., Kauzlarich, S. M. & Sutter, E. (2006). *Langmuir*, **22**, 5455–5458.
- Chou, N. H., Oyler, K. D., Motl, N. E. & Schaak, R. E. (2009). *Chem. Mater.* **21**, 4105–4107.
- Cosentino, S., Sungur Ozen, E., Raciti, R., Mio, A. M., Nicotra, G., Simone, F., Crupi, I., Turan, R., Terrasi, A., Aydinli, A. & Mirabella, S. (2014). *J. Appl. Phys.* **115**, 043103.
- D'Angelo, P. & Migliorati, V. (2015). *J. Phys. Chem. B*, **119**, 4061–4067.
- Ferrer, D., Blom, D. A., Allard, L. F., Mejía, S., Pérez-Tijerina, E. & José-Yacamán, M. (2008). *J. Mater. Chem.* **18**, 2442–2446.
- Filippini, A. & Di Cicco, A. (1995). *Phys. Rev. B*, **51**, 12322–12336.
- Frenkel, A. I. (1999). *J. Synchrotron Rad.* **6**, 293–295.
- Girod, M., Vogel, S., Szczerba, W. & Thünemann, A. F. (2015). *J. Magn. Magn. Mater.* **380**, 163–167.
- Henderson, E. J., Seino, M., Puzzo, D. P. & Ozin, G. A. (2010). *ACS Nano*, **4**, 7683–7691.
- Hope-Weeks, L. J. (2003). *Chem. Commun.* pp. 2980–2981.
- Hyun, S. P. & Hayes, K. F. (2015). *Appl. Clay Sci.* **107**, 122–130.
- Jia, C., Liu, Q., Sun, C.-J., Yang, F., Ren, Y., Heald, S. M., Liu, Y., Li, Z.-F., Lu, W. & Xie, J. (2014). *Appl. Mater. Interfaces*, **6**, 17920–17925.
- Joly, Y. (2001). *Phys. Rev. B*, **63**, 125120.
- Kabi, S. & Perera, A. G. U. (2015). *J. Appl. Phys.* **117**, 124303.
- Kairdolf, B. A., Smith, A. M., Stokes, T. H., Wang, M. D., Young, A. N. & Nie, S. (2013). *Annu. Rev. Anal. Chem.* **6**, 143–162.
- Karatutlu, A., Song, M., Wheeler, A. P., Ersoy, O., Little, W. R., Zhang, Y., Puech, P., Boi, F. S., Luklinska, Z. & Sapelkin, A. V. (2015). *RSC Adv.* **5**, 20566–20573.
- Ke, R., Zhang, X., Wang, L., Zhang, C., Zhang, S., Niu, H., Mao, C., Song, J., Jin, B. & Tian, Y. (2015). *J. Solid State Electrochem.* **19**, 1633–1641.
- Kim, J. Y., Voznyy, O., Zhitomirsky, D. & Sargent, E. H. (2013). *Adv. Mater.* **25**, 4986–5010.
- Kolobov, A. V., Oyanagi, H., Frenkel, A., Robinson, I., Cross, J., Wei, S., Brunner, K., Abstreiter, G., Maeda, Y., Shklyav, A., Ichikawa, M., Yamasaki, S. & Tanaka, K. (2003). *Nucl. Instrum. Methods Phys. Res. B*, **199**, 174–178.
- Kolobov, A. V., Oyanagi, H., Maeda, Y. & Tanaka, K. (2001). *J. Synchrotron Rad.* **8**, 511–513.
- Kolobov, A. V., Wei, S. Q., Yan, W. S., Oyanagi, H., Maeda, Y. & Tanaka, K. (2003). *Phys. Rev. B*, **67**, 195314.
- Lee, D. C., Pietryga, J. M., Robel, I., Werder, D. J., Schaller, R. D. & Klimov, V. I. (2009). *J. Am. Chem. Soc.* **131**, 3436–3437.
- Little, W., Karatutlu, A., Bolmatov, D., Trachenko, K., Sapelkin, A. V., Cibir, G., Taylor, R., Mosselmann, F., Dent, A. J. & Mountjoy, G. (2014). *Sci. Rep.* **4**, 7372.
- Lu, K. (2012). *Nanoparticulate Materials: Synthesis, Characterization and Processing*. New Jersey: John Wiley and Sons.
- Lv, P., Chen, Z., Zhang, A. H. X. & IEEE (2009). *Effect of Laser Annealing on amorphous Silicon Carbide Films Prepared by PECVD, 4th IEEE International Conference of Nano/Micro Engineered and Molecular Systems*, pp. 743–746.
- Mao, L. F. (2013). *Nanoscale Res. Lett.* **8**, 369.
- Marcins, G., Butikova, J., Tale, I., Polyakov, B., Kalendarjov, R. & Muhin, A. (2011). *IOP Conf. Ser.: Mater. Sci. Eng.* **23**, 012035.
- Michalet, X., Pinaud, F. F., Bentolila, L. A., Tsay, J. M., Doose, S., Li, J. J., Sundaresan, G., Wu, A. M., Gambhir, S. S. & Weiss, S. (2005). *Science*, **307**, 538–544.
- Moore, C. A., Rocca, J. J., Johnson, T., Collins, G. J. & Russell, P. E. (1983). *Appl. Phys. Lett.* **43**, 290–292.
- Muthuswamy, E., Iskandar, A. S., Amador, M. M. & Kauzlarich, S. M. (2013). *Chem. Mater.* **25**, 1416–1422.
- Nelmes, R. J., McMahon, M. I., Wright, N. G., Allan, D. R. & Loveday, J. S. (1993). *Phys. Rev. B*, **48**, 9883–9886.
- Newville, M. (2014). *Reviews in Mineralogy and Geochemistry*, Vol. 78, *Spectroscopic Methods in Mineralogy and Materials Sciences*, edited by G. S. Henderson, D. R. Neuville and R. T. Downs, pp. 33–74.
- Norman, D. (1986). *J. Phys. C*, **19**, 3273–3311.
- Pal, S. K. (2015). *Carbon*, **88**, 86–112.
- Pellegrino, T., Kudera, S., Liedl, T., Muñoz Javier, A., Manna, L. & Parak, W. J. (2005). *Small*, **1**, 48–63.
- Peng, X., Long, Q., Li, H., Zhang, Y. & Yao, S. (2015). *Sens. Actuators B*, **213**, 131–138.
- Peng, W., Sampat, S., Rupich, S. M., Anand, B., Hue Minh, N., Taylor, D., Beardon, B. E., Gartstein, Y. N., Chabal, Y. J. & Malko, A. V. (2015). *Nanoscale*, **7**, 8524–8530.
- Penner-Hahn, J. E. (2002). *Abstr. Pap. Am. Chem. Soc.* **224**, U149.
- Pin, S., Le Tilly, V., Alpert, B. & Cortes, R. (1989). *FEBS Lett.* **242**, 401–404.
- Pizzagalli, L. & Galli, G. (2002). *Mater. Sci. Eng. B*, **96**, 86–89.
- Pizzagalli, L., Galli, G., Klepeis, J. E. & Gygi, F. (2001). *Phys. Rev. B*, **63**, 165324.
- Priebe, J. B., Radnik, J., Lennox, A. J. J., Pohl, M.-M., Karnahl, M., Hollmann, D., Grabow, K., Bentrup, U., Junge, H., Beller, M. & Brückner, A. (2015). *ACS Catal.* **5**, 2137–2148.
- Qian, Z. S., Chai, L. J., Huang, Y. Y., Tang, C., Jia Shen, J., Chen, J. R. & Feng, H. (2015). *Biosens. Bioelectron.* **68**, 675–680.
- Ravel, B., Newville, M., Cross, J. O. & Bouldin, C. E. (1995). *Physica B*, **208–209**, 145–147.
- Resch-Genger, U., Grabolle, M., Cavaliere-Jaricot, S., Nitschke, R. & Nann, T. (2008). *Nat. Methods*, **5**, 763–775.
- Robel, I., Shabaev, A., Lee, D. C., Schaller, R. D., Pietryga, J. M., Crooker, S. A., Efros, A. L. & Klimov, V. I. (2015). *Nano Lett.* **15**, 2685–2692.
- Rockenberger, J., Tröger, L., Kornowski, A., Vossmeier, T., Eychmüller, A., Feldhaus, J. & Weller, H. (1997). *J. Phys. Chem. B*, **101**, 2691–2701.
- Ryu, S.-G., Gruber, I., Grigoropoulos, C. P., Poulidakos, D. & Moon, S.-J. (2012). *Thin Solid Films*, **520**, 6724–6729.
- Samavati, A., Mustafa, M. K., Othaman, Z. & Ghoshal, S. K. (2015). *J. Nanomater.* **2015**, 681242.
- Samavati, A., Othaman, Z., Ghoshal, S. K. & Mustafa, M. K. (2015). *Chin. Phys. B*, **24**, 028103.
- Sanehira, E. M., Tu, C.-C. & Lin, L. Y. (2012). *2012 IEEE Photonics Conference (Ipc)*, pp. 386–387.

- Scarselli, M., Masala, S., Castrucci, P., De Crescenzi, M., Gatto, E., Venanzi, M., Karmous, A., Szkutnik, P. D., Ronda, A. & Berbezier, I. (2007). *Appl. Phys. Lett.* **91**, 141117.
- Selli, D., Baburin, I. A., Martoňák, R. & Leoni, S. (2013). *Sci. Rep.* **3**, 1466.
- Stern, E. A., Bouldin, C. E., von Roedern, B. & Azoulay, J. (1983). *Phys. Rev. B*, **27**, 6557–6560.
- Sun, K. W., Sue, S. H. & Liu, C. W. (2005). *Physica E*, **28**, 525–530.
- Sun, L., Gong, F., Zhou, C., Wang, H. & Yao, S. (2015). *Mater. Express*, **5**, 219–225.
- Sun, Y., Frenkel, A. I., Isseroff, R., Shonbrun, C., Forman, M., Shin, K. W., Koga, T., White, H., Zhang, L. H., Zhu, Y. M., Rafailovich, M. H. & Sokolov, J. C. (2006). *Langmuir*, **22**, 807–816.
- Sun, Z. H., Wei, S. Q., Kolobov, A. V., Oyanagi, H. & Brunner, K. (2005). *Phys. Rev. B*, **71**, 245334.
- Toko, K., Numata, R., Oya, N., Fukata, N., Usami, N. & Suemasu, T. (2014). *Appl. Phys. Lett.* **104**, 022106.
- Tseng, W., Dietrich, H., Davey, J., Christou, A. & Anderson, W. T. (1980). *J. Electron. Mater.* **9**, 685–692.
- Uesugi, H., Kita, M. & Omata, T. (2015). *J. Cryst. Growth*, **416**, 134–141.
- Vaughn, D. D. II, Bondi, J. F. & Schaak, R. E. (2010). *Chem. Mater.* **22**, 6103–6108.
- Weber, J. R., Janotti, A. & Van de Walle, C. G. (2013). *Phys. Rev. B*, **87**, 035203.
- Weeks, J. D. & Gilmer, G. H. (2007). *Advances in Chemical Physics*, pp. 157–228. New York: John Wiley and Sons.
- Wheeler, L. M., Levij, L. M. & Kortshagen, U. R. (2013). *J. Phys. Chem. Lett.* **4**, 3392–3396.
- Wolf, O., Dasog, M., Yang, Z., Balberg, I., Veinot, J. G. C. & Millo, O. (2013). *Nano Lett.* **13**, 2516–2521.
- Wong, K. M. (2009). *Jpn. J. Appl. Phys.* **48**, 085002.
- Wu, J., Sun, Y., Zou, R., Song, G., Chen, Z., Wang, C. & Hu, J. (2011). *CrystEngComm*, **13**, 3674–3677.
- Yakimov, A. I., Kirienko, V. V., Armbrister, V. A. & Dvurechenskii, A. V. (2014). *Semicond. Sci. Technol.* **29**, 085011.
- Yuryev, V. A., Arapkina, L. V., Storozhevikh, M. S., Chapnin, V. A., Chizh, K. V., Uvarov, O. V., Kalinushkin, V. P., Zhukova, E. S., Prokhorov, A. S., Spektor, I. E. & Gorshunov, B. P. (2012). *Nanoscale Res. Lett.* **7**, 414.
- Zaitseva, N., Dai, Z. R., Grant, C. D., Harper, J. & Saw, C. (2007). *Chem. Mater.* **19**, 5174–5178.
- Zhang, R.-Q., De Sarkar, A., Niehaus, T. A. & Frauenheim, T. (2012). *Phys. Status Solidi B*, **249**, 401–412.
- Zhang, X. X., Jin, Y. X., Ye, X. S., Wang, C. & Yang, Y. (2014). *Acta Phys. Sin.* **63**, 156802.
- Zhang, Y., Karatutlu, A., Ersoy, O., Little, W., Cibin, G., Dent, A. & Sapelkin, A. (2015). *J. Synchrotron Rad.* **22**, 105–112.
- Zhou, H., Zhou, G., Zhou, J., Xu, D., Zhang, X., Kong, P. & Yang, Z. (2015). *Mater. Res. Bull.* **65**, 53–60.